ACS Partner Journal

PRECISION CHEMISTRY

Editors' Choice

Open Access

pubs.acs.org/PrecisionChem

Article

Disentangling Multiple pH-Dependent Factors on the Hydrogen Evolution Reaction at Au(111)

Published as part of Precision Chemistry special issue "Precision Chemistry for the Hydrogen Cycle".

Er-Fei Zhen, Bing-Yu Liu, Meng-Ke Zhang, Lu−Lu Zhang, Chen-Yu Zhang, Jun Cai, Marko M. Melander, Jun Huang,* and Yan-Xia Chen*

Cite This: *Precis. Chem.* 2025, 3, 135−148

Read Online

ACCESS | Metrics & More | Article Recommendations | Supporting Information

ABSTRACT: Understanding how the electrolyte pH affects electrocatalytic activity is a topic of crucial importance in a large variety of systems. However, unraveling the origin of the pH effects is complicated often by the fact that both the reaction driving forces and reactant concentrations in the electric double layer (EDL) change simultaneously with the pH value. Herein, we employ the hydrogen evolution reaction (HER) at Au(111)-aqueous solution interfaces as a model system to disentangle different pH-dependent factors. In 0.1 M NaOH, the HER current density at Au(111) in the potential range of −0.4 V < E_{RHE} < 0 V is up to 60 times smaller than that in 0.1 M $HClO_4$. A reaction model with proper consideration of the local reaction conditions within the EDL is developed. After correcting for the EDL effects, the rate constant for HER is only weakly pH-dependent. Our analysis unambiguously reveals that the observed pH effects are mainly due to the pH-dependent reorganization free energy, which depends on the electrostatic potential and the local reaction conditions within the EDL. Possible origins of the pH and temperature dependence of the activation energy and the electron transfer coefficients are discussed. This work suggests that factors influencing the intrinsic pH-dependent kinetics are easier to understand after proper corrections of EDL effects.

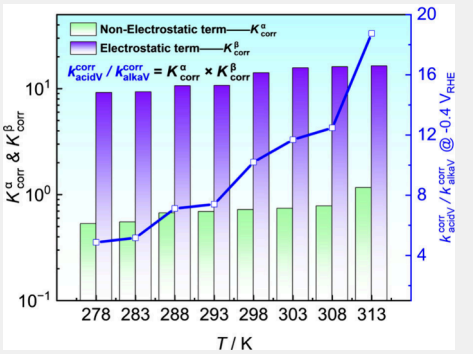

KEYWORDS: *hydrogen evolution reaction, Au(111) electrode, pH effect, rate constants, EDL effects*

1. INTRODUCTION

Most electrochemical energy conversion technologies involve complex electrode reactions with multiple pathways (even multiple products). Furthermore, each pathway usually includes multiple elementary steps but already the kinetics of a single elementary step may depend on multiple, intertwined factors such as catalytic effects (adsorbate bonding energy, coverage, reaction barrier), solvent effects, electric double layer (EDL) effects, mass transport effects and so on. Reliably quantifying the contribution of the various factors on the elementary reaction kinetics is of great importance in establishing the principles of electrocatalysis and unravelling the key factors controlling the overall kinetics of complex reactions. Being the simplest electrocatalytic reaction, hydrogen evolution reaction (HER) has served as the prototypical model reaction for more than a century and hence holds a pivotal role in the development of theories in electrocatalysis.[1−3] The HER has helped in the formulation of the Butler−Volmer rate law[4−6] and the slow discharge theory[7] of electrode kinetics in the 1920s and 1930s, the establishment of the binding energy approach in electrocatalysis in the 1970s,[8] as well as the development of the computational hydrogen electrode method in the 2000s.[9]

Although HER involves the transfer of only two protons and two electrons, a complete understanding of factors influencing its reaction mechanism and kinetics has not been reached yet. For example, studies on various electrocatalysts have confirmed that HER current density in acid is ca. 1 to 3 orders of magnitude higher than that in alkali.[10−13] However, the origin(s) of pH-dependent HER activity has been hotly debated in past decades,[14−16] and several reasons have been proposed: (i) increase in the binding energy of hydrogen (HBE) with pH;[17−21] (ii) change in the nature of the proton donor from H_3O^+ in acid to H_2O in alkali;[22−25] (iii) changes in double layer structure, electric field and entropy factor;[26−28] (iv) changes in the hydrogen bond network connectivity within the EDL.[29,30] The understanding of the pH effect on HER has undergone an intriguing shift. The perspective gradually transitioned from the view of Yan and Goddard et.al, who focused on the changes in

Received: October 3, 2024
Revised: December 17, 2024
Accepted: December 17, 2024
Published: January 8, 2025

https://doi.org/10.1021/prechem.4c00081
Precis. Chem. 2025, 3, 135−148

metal−hydrogen bond strength with pH in heterogeneous catalysis,[18,19] to the approach of Karen Chan and Markovic et.al, who considered the changes in reactants with pH.[12,23,25] Currently, the focus has shifted to the perspective of Koper, Chen and others, who emphasize changes in the double layer structure and electric field with pH.[28,29] However, the study of EDL effects on electrode kinetics is not new and can be traced back to the 1930s.[7] Scholars, represented by Frumkin, gradually deepened their understanding through the study of HER on Hg and the reduction of peroxydisulfate anion, and proposed theories such as the Frumkin correction, which is now nearly a century old.[1,31,32] However, there is a risk that such excellent theories have been forgotten in the past two or three decades. Recently, some electrolyte effects in electrocatalytic reactions represented by oxygen evolution, carbon dioxide reduction, and formic acid oxidation, such as pH effects and cation effects, have been re-emphasized by researchers for their influence of the EDL effect on electrode kinetics.[33−35] Increasing attention is being directed toward the role of the EDL region in influencing the kinetics of electrocatalytic reactions.[33,36,37]

Despite progress, a fully satisfactory and concise description of pH-dependency even in the simplest electrocatalytic reaction, HER, has not been reached due to challenges met in unveiling the underlying causes of the pronounced decrease in the HER current with increasing pH. The following challenges can be identified: (i) Most data on the pH-dependent activity of HER were obtained for platinum-group metals (PGMs), particularly Pt-based electrocatalysts,[17,28,38−41] but the HER mechanism on such catalysts is different in acidic and alkaline media.[41,42] (ii) the most commonly used the activity metric, i.e., the exchange current density or current density at fixed overpotential, does not reflect the intrinsic reaction kinetics because it also includes the influence of reactant concentrations and adsorbate coverage in addition to the rate constant.[43] Therefore, the observed differences in the HER activity results from the interplay of multiple factors, including electronic interactions between intermediate adsorbates and electrode materials, electrostatic interactions within the EDL and so on.

Compared to Pt-based electrocatalysts, less active metals, such as gold, possess several advantages in mechanistic investigations of pH effects on the HER. First, at these less active catalysts, such as coinage metals,[44,45] the first electron transfer step, i.e., the Volmer step, is the rate-determining step (RDS) of HER in both acidic and alkaline solutions. Second, it is anticipated that the EDL effects are more pronounced for such mediocre catalysts. Lastly, the kinetic parameters, such as the activation energy (E_a) and the pre-exponential factor (A), can be determined more accurately since the complications from the second elementary step can be eliminated.[44]

For these reasons, the HER at the Au(111) electrode is taken as the model reaction in this study and herein we report our results from our systematic studies on the pH and temperature effects on HER kinetics in 0.1 M $HClO_4$ and NaOH solutions. A multiscale and multiphase EDL model considering mass transfer with steric effect, EDL structure and electrocatalytic reaction, is utilized to obtain microscopic and macroscopic insight on the local reaction conditions and their effect on the HER current. We perform a quantitative analysis of multiple factors on the pH-dependent HER kinetics and have determined the (standard) activation Gibbs free energy, charge transfer coefficient for the Volmer reaction as well as their potential, pH and temperature dependencies. The origins of the difference in HER kinetics at Au(111) in acidic and alkaline media are discussed. The apparent pH effects observed, i.e., ca. 1 to 60 times difference in HER current density are primarily due electrostatic effects leading to alterations in the concentration of reactants and the electric potential at the reaction plane within the EDL between acidic and alkaline environments. Possible origins of differences in the activation energy and charge transfer coefficients, their temperature dependence in acid and alkaline media as well as their correlation with temperature dependent change of solvent reorganization free energy, will be discussed.

2. EXPERIMENTAL METHOD

Gold (111) single crystals electrodes were prepared according to Clavilier's[46] method and used as the working electrode (WE). The reference electrode, saturated calomel electrode (SCE), was maintained at room temperature and connected to the cell through a long Luggin capillary. An Au wire was used as the counter electrode (CE). The electrolyte solutions, i.e.,0.1 M $HClO_4$ and 0.1 M NaOH, were prepared using perchloric acid (70% ∼ 72%, Aladdin), sodium hydroxide (99.99%, Sigma-Aldrich) and ultrapure water (18.2 MΩ cm, Milli-Q pure water system). During the measurements, the electrolyte was constantly purged with Ar (99.999%, Nanjing Special Gas Corp.). Before the measurements, the solution was purged with Ar for at least 20 min. All glassware was boiled three times with a cleaning solution of ultrapure water to thoroughly remove trace impurities.

Before each experiment, the single crystal electrode was flame-annealed followed by quenching in ultrapure water (18.2 MΩ cm). During the transfer of the WE to the electrochemical cell, the electrode surface was protected with ultrapure water to prevent contamination by airborne impurities. The electrode surface was covered with deoxygenated water droplets during the transfer to the electrochemical cell to avoid contact with impurities. During all measurements, the meniscus configuration was maintained between the WE surface and the electrolyte. A thermostatic cell was used in all experiments on temperature effects, and the cell temperature was controlled by water flow from the thermo-bath at the desired temperature through a glass jacket. The experiments were carried out at various temperatures in the range 278 K $\leq T \leq$ 313 K with an accuracy of ±0.1 K.

The electrode was continuously cycled in the potential region from 0 to 1.2 V_{RHE} at a scan rate of 50 mV/s until clean and reproducible cyclic voltammetry (CV) curves were obtained. Then, the HER $j-E$ curves at the corresponding temperatures were recorded in the hanging-meniscus rotating disk electrode (HMRDE) configuration with a rotation speed of 3600 rpm. The Ohmic resistance between the working electrode and the Luggin capillary of the reference electrode was measured by electrochemical impedance spectrometry and then compensated (to 95%) at each temperature.[47] The currents were normalized to the geometric surface areas of the WE to obtain the current density. To compare experimental data at the same overpotential, all potentials measured at any temperature were converted to the RHE scale after correction of the thermal junction potential.[48] To ensure that the crystallinity of the Au(111) electrode did not change significantly during the experiments, the electrode was reannealed before each temperature and the quality of Au(111) electrode as well as the cleanness of the cell system was checked by CV before recording the $j-E$ curves for HER (Figures S3 and S4).

3. MODEL DEVELOPMENT

We model the reduction of hydronium and water molecules at Au(111) in 0.1 M $HClO_4$ and 0.1 M NaOH electrolyte from 278 to 313 K, respectively, to understand the pH and temperature effects on the HER. The total model connects a microkinetic submodel and an EDL submodel, from which the electric potential and concentration distribution within the EDL can be obtained.

https://doi.org/10.1021/prechem.4c00081
Precis. Chem. 2025, 3, 135−148

3.1. Reaction Mechanism

In an acidic solution, hydrated protons (H^+) are the discharging precursor. The overall reaction for HER in acidic medium is

$$2H^+ + 2e^- \rightleftharpoons H_2 \quad (R1)$$

which proceeds via the following elementary steps:

$$\text{Volmer step: } H^+ + {}^* + e^- \rightleftharpoons H_{ad} \quad (R2)$$

$$\text{Heyrovsky step: } H^+ + H_{ad} + e^- \rightleftharpoons H_2 + {}^* \quad (R3)$$

$$\text{Tafel step: } 2H_{ad} \rightleftharpoons H_2 + 2^* \quad (R4)$$

In alkaline medium, water molecules are the hydrogen donors and the overall HER mechanism is

$$2H_2O + 2e^- \rightleftharpoons H_2 + 2OH^- \quad (R5)$$

with the following elementary steps:

$$\text{Volmer step: } H_2O + {}^* + e^- \rightleftharpoons H_{ad} + OH^- \quad (R6)$$

$$\text{Heyrovsky step: } H_2O + H_{ad} + e^- \rightleftharpoons H_2 + OH^- + {}^* \quad (R7)$$

$$\text{Tafel step: } 2H_{ad} \rightleftharpoons H_2 + 2^* \quad (R8)$$

3.2. Kinetic Rate Equation

The Volmer step is assumed to be the rate-determining step (RDS) of the HER at Au(111) in acidic (R2) and alkaline solutions (R6).[44] As HER takes place on or near the surface, only hydrated protons or water molecules within a certainty distance from the surface or within a certain space of the EDL contribute to the reaction.[49,50] For simplicity, we assume that the all hydrogen donation takes place at the most likely reaction plane (RP), which is located near the inner Helmholtz plane of the EDL. Since the Volmer reaction is the rate-determining step of HER, the coverage of H_{ad} at Au(111) is nearly zero, we can safely ignore the backward reaction and the HER rate is

$$j_{acid} = 2j_{2f} = -2e_0 n_M \frac{c_{H^+}^{RP}}{c_{H^+}^{0}} A \exp\left(-\frac{\Delta G_{acidV}^{\neq}(E_{SHE})}{RT}\right) \quad (1)$$

in 0.1 M $HClO_4$ solution, and

$$j_{alka} = 2j_{6f} = -2e_0 n_M \frac{c_{H_2O}^{RP}}{c_{H_2O}^{0}} A \exp\left(-\frac{\Delta G_{alkaV}^{\neq}(E_{SHE})}{RT}\right) \quad (2)$$

in 0.1 M NaOH solution. The j_{2f}/j_{6f} specifically refers to the current density of forward acid/alkaline Volmer step (R2/R6) of the HER. A is the pre-exponential factor; the superscript RP denotes the reaction plane, $c_{H^+}^{RP}$ and $c_{H_2O}^{RP}$ represent the concentration of protons and water at the RP, n_M is the number density of Au atoms on Au(111) electrode, R is the gas constant, and T is the absolute temperature. e_0 is the elementary charge, $c_{H^+}^{0}$ and $c_{H_2O}^{0}$ are the concentrations of hydronium and water under standard conditions, respectively. Because water molecules are uncharged and their concentration is significantly higher than other solution-phase species, we assume that $c_{H_2O}^{RP} = c_{H_2O}^{bulk}$. $\Delta G_{acidV}^{\neq}(E_{SHE})$ and $\Delta G_{alkaV}^{\neq}(E_{SHE})$ are the activation energies of the Volmer step of hydronium and water discharge both of which are functions of the applied electrode potential (E_{SHE}). Assuming that the reaction barrier follows to the Brønsted-Evans−Polanyi relation,[51] it gives

$$\Delta G_{acidV}^{\neq}(E_{SHE}) = \Delta G_{acidV}^{\neq,0} + \alpha_{acidV} F(E_{SHE} - \phi_{acid}^{RP} - E_{SHE,acidV}^{0}) \quad (3)$$

$$\Delta G_{alkaV}^{\neq}(E_{SHE}) = \Delta G_{alkaV}^{\neq,0} + \alpha_{alkaV} F(E_{SHE} - \phi_{alka}^{RP} - E_{SHE,alkaV}^{0}) \quad (4)$$

where $\Delta G_{acidV}^{0,\neq}$ and $\Delta G_{alkaV}^{0,\neq}$ are the equilibrium activation energies of the Volmer reaction with hydronium and water molecule, respectively, as the discharge precursor. α_{acidV} and α_{alkaV} are the corresponding charge transfer coefficients. According to the general definition of electrode potentials,[52] the applied electrode potential (E_{SHE}) can be written as $E_{SHE} = \phi_M - \phi_S - \mu_e^M/F - E_{abs}^{SHE}$, where ϕ_M and ϕ_S are the inner electric potential of the metal electrode and the solution, μ_e^M is the chemical potential of electrons in the metal electrode, which can be estimated from DFT calculations,[53,54] and E_{abs}^{SHE} is the absolute potential of the standard hydrogen electrode (SHE). ϕ_{acid}^{RP} and ϕ_{alka}^{RP} are the electric potentials at the RP under acidic and alkaline media, respectively. $E_{SHE,\,acidV}^{0}$ and $E_{SHE,\,alkaV}^{0}$ are the standard equilibrium potentials of the Volmer step in acidic and alkaline conditions. Because of the low coverage of adsorbed hydrogen at the Au(111) within the potential range of interest, their impacts on the later interactions and reaction barrier are ignored.

3.3. EDL Model

Since the local reactant (H^+) and product (OH^-) concentrations and reaction barriers depend on the electric potentials at the RP, the concentration of ionic species involved in electrochemical reactions n_i (i = H^+, Na^+, OH^-, ClO_4^-) and the distribution of the electric potential ϕ across the EDL are needed. We determine them by solving the modified Poisson-Nernst−Planck (PNP) equation, considering diffusion, electromigration as well as steric effects.[36,57,58]

$$\frac{\partial}{\partial x}\left(\epsilon_s \frac{\partial \phi}{\partial x}\right) = -e_0 \sum z_i n_i \quad (5)$$

$$\frac{\partial n_i}{\partial t} = \frac{\partial}{\partial x}\left(D_i \frac{n_s}{n_t}\frac{\partial n_i}{\partial x} + D_i \frac{n_i}{n_t}\frac{\gamma_i}{\gamma_s}\sum_{j\neq s}\frac{\gamma_j}{\gamma_s}\frac{\partial n_j}{\partial x} + \frac{D_i}{k_B T}\frac{n_s}{n_t} n_i z_i e_0 \frac{\partial \phi}{\partial x}\right) \quad (6)$$

where ϵ_s is the dielectric permittivity of the bulk aqueous solution, z_i, n_i, and D_i are the charge number, number density, and diffusion coefficient of ion i, respectively. n_s is the number density of water molecules, n_t is the total number density. $\gamma_i = (d_i/d_t)^3$ is the size coefficient accounting for finite size effects, with d_i being length of the cubic cell occupied by particle i, and d_t being the reference size. k_B is the Boltzmann constant.The symbol $j \neq s$ denotes ions in the electrolyte solution other than water molecules.

Solving this set of partial differential eqs 5 and 6) requires the initial and the left and right boundary conditions. The RP is defined as the left boundary at $x = 0$ and the left boundary conditions are

$$J_i = \upsilon_i \frac{j_{HER}}{n e_0} \quad (7)$$

https://doi.org/10.1021/prechem.4c00081
Precis. Chem. 2025, 3, 135−148

$$\phi(0, t) = \phi_M - \chi_M - \left(-\frac{\partial\phi}{\partial x}(0, t)\delta_{RP}\frac{\epsilon_s}{\epsilon_{RP}}\right) \quad (8)$$

Equation 7 is the Faraday's law of electrolysis, which relates the reactant and product fluxes (J_i) with the total current density of the reaction (j_{HER}). n is the number of electrons transferred during the HER, and υ_i is the stoichiometric number of ion i, which equals 0 if it does not participate in the electrochemical reaction. χ_M is the surface potential of the metal-solution interface.$-\frac{\partial\phi}{\partial x}(0, t)\delta_{RP}\frac{\epsilon_s}{\epsilon_{RP}}$ represents the electric potential drop in the compact layer of EDL attributed to the surface free charge, δ_{RP} is the distance from the metal surface to the RP, and ϵ_{RP} is the dielectric permittivity of the space between the metal and the RP. The value of $\epsilon_{RP} = 6\,\epsilon_0$ used at 298 K in this work, are closed to this used by Parsons.[59]

The right boundary corresponds to the bulk solution at $x = x_b$ with the boundary conditions

$$n_i(x_b, t) = n_i^b \quad (9)$$

$$\phi(x_b, t) = 0 \quad (10)$$

The initial conditions at $t = 0$ are

$$n_i(x, 0) = n_i^b \quad (11)$$

$$\phi(x, 0) = 0 \quad (12)$$

A schematic illustration of the potential distribution and the corresponding ion distribution at the Au(111)/electrolyte interface at potentials where the HER occurs is shown in Figure 1. On the Au(111) electrode HER takes place in a potential region where the surface free charge density is always negative because the potential of zero free charge (PZFC) of Au(111) in 0.1 M $HClO_4$ solution is ca. 0.53 V_{SHE},[60] which is higher than the potential region where HER occurs. The RP is located at $x = 0$, which is also the minimum ion-surface distance. Beyond the RP lies the diffuse layer, whose characteristic thickness is about Debye length[61] $\lambda_D = \sqrt{k_B T\varepsilon_s/2e_0^2 n^b} \approx 1.5$ nm in this work. The diffusion layer thickness can be estimated from the Levich theory of rotation disk electrodes

$$\delta_D = 1.61 D^{1/3}\nu^{1/6}\omega^{-1/2} \quad (13)$$

where D is the reference diffusion coefficient, ν is the kinematic viscosity of the solution phase, and ω is the rotation speed of the rotating disk electrode apparatus. We consider the effect of convection by limiting the thickness of the diffusion layer.

As shown in Figure S1, we solve the PNP equation, eqs 5-6, in MATLAB, with the boundary conditions, eqs 7-10, and initial conditions, eqs 11-12. The numerical solutions provide the potential-dependent concentration and potential distributions. The current can be obtained by solving eq 1 and eq 2. Note that the current is related to the flux through eq 7, which is the left boundary of the PNP equation. Therefore, we coupled these two parts to ensure that the results are self-consistent and convergent. The temperature-independent parameters are given in Table S1, and the temperature-dependent parameters are listed in Table S2. Figure S2 illustrates the variation in hydronium concentration and electric potential within the double layer, corresponding to the applied electrode potential, in solutions of 0.1 M $HClO_4$ and 0.1 M NaOH.

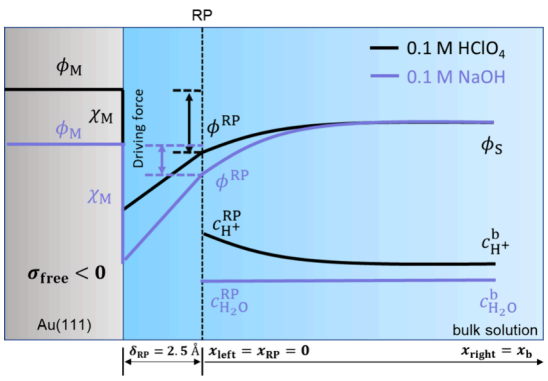

Figure 1. Schematic illustration of the distribution of electric potential and the concentration of reactants in the EDL of Au(111) in 0.1 M $HClO_4$ (black lines) and NaOH (baby blue lines) under HER conditions at the same overpotential, where the surface free charge on the Au(111) surface $\sigma_{free} < 0$ and the electrostatic potential difference between the metal and solvent, $\phi_M - \phi_S < \chi_M$, with ϕ_M and ϕ_S being the inner electric potential of the metal electrode and the solution, and χ_M being the surface potential of the metal-solution interface due to spill over of electrons. The RP is the reaction plane, located near the inner Helmholtz plane of the EDL with a distance of ca. 2.5 Å to the Au(111) surface.[29,55,56] The RP is used as the left boundary of the modified Poisson−Nernst−Planck (PNP) equation ($x_{left} = x_{RP} = 0$). The bulk solution is used as the right boundary ($x_{right} = x_b$). The driving force is calculated by $\phi_M - \phi^{RP}$, where ϕ^{RP} is the inner electric potential at the RP. Due to electrostatic attraction, the concentration of the hydronium ion at the RP is higher than that of the bulk solution ($c_{H^+}^{RP} > c_{H^+}^b$). Since the water molecule is uncharged, its concentration at the RP is equal to the bulk concentration ($c_{H_2O}^{RP} = c_{H_2O}^b$).

4. RESULTS AND DISCUSSION

4.1. Experimental Polarization Curves of HER at Au(111) and Model Analysis

Two representative sets of the j−E curves for HER at Au(111) recorded in 0.1 M $HClO_4$ and 0.1 M NaOH solutions at different temperatures from 278 to 313 K are displayed in Figure 2A and 2B. The HER current at Au(111) increases with rising temperature, suggesting that the HER at the Au(111) electrode is an activated process. With increasing temperature, the Tafel slope in the low overpotential region decreases from 108 to 89 mV/dec in 0.1 M $HClO_4$ (Figure 2C) and from 175 to 120 mV/dec in 0.1 M NaOH solutions (Figure 2D), respectively. This corresponds to an increase in the apparent charge transfer coefficient (α_{app}) from ca. 0.51 to 0.68 in acidic solution and from 0.32 to 0.52 in basic solution with the increase in temperature from 278 to 313 K. The smaller α_{app} in alkaline media than that in acidic media has been previously observed for HER on pc-Au in unbuffered and buffered solutions.[62,63] The temperature dependency also aligns with previous reports on HER at metal electrodes such as Ag, Au and Hg.[64,65] A similar pH-dependency of HER at Pt group metals has also been reported and the apparent HER current at the same potential on the RHE scale in acidic media is higher than that in alkaline media.[28,39,41]

The ratio of the HER current density in acid and in base at the same E_{RHE}, $r_j(E_{RHE}) = j_{0.1MHClO_4}/j_{0.1MNaOH}$, is presented as a function of potential in Figure 4A. At the same temperature, r_j increases at more negative electrode potentials. At the same E_{RHE}, r_j rises with increasing temperature. In the potential range with $-0.4\ V < E_{RHE} < -0.1\ V$, r_j is in the range from 1 to ca. 60, depending on the applied potential and the temperature.

https://doi.org/10.1021/prechem.4c00081
Precis. Chem. 2025, 3, 135−148

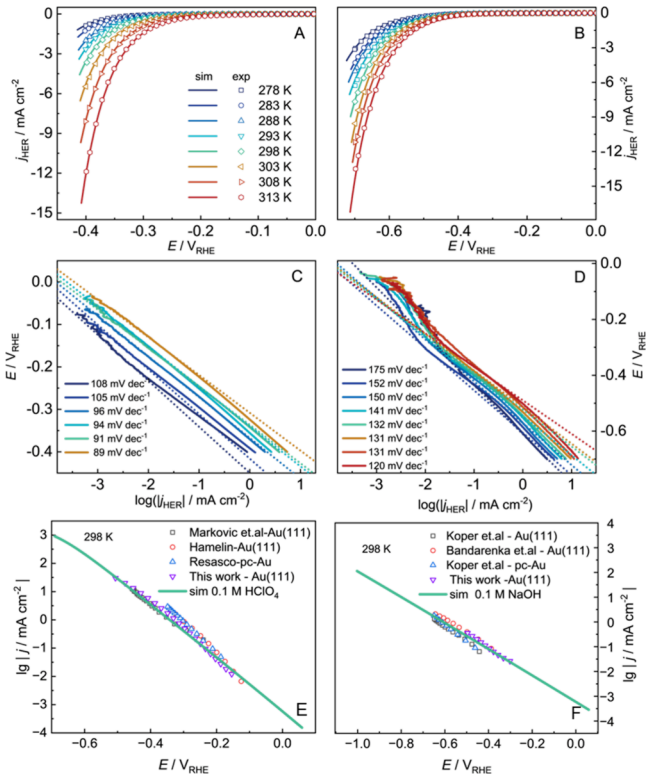

Figure 2. Simulated (solid lines) and measured (dots) j–E curves for HER at the Au(111) electrode in Ar-saturated (A) 0.1 M $HClO_4$ and (B) 0.1 M NaOH solutions at various temperatures. The j–E curves are automatically recorded with 95% Ohmic compensation. The potential scan rate was 10 mV/s, and the electrode rotation speed is 3600 rpm. (C–D) The corresponding Tafel plots of HER in (C) 0.1 M $HClO_4$ at 278–303 K and (D) 0.1 M NaOH at 278–313 K. (E) Simulated (solid lines) and measured (different dots) j–E curves for HER at Au(111) electrode or polycrystalline Au at 298 K in 0.1 M $HClO_4$ solution. Experimental data come from refs 66–68. (F) Simulated (solid lines) and measured (different dots) j–E curves for HER at the Au(111) electrode or polycrystalline Au at 298 K in 0.1 M NaOH solution. Experimental data come from refs 69–71.

In order to disentangle the catalytic and electrostatic effects on HER kinetics, the potential dependent HER current density at Au(111) in acidic media on the SHE scale is expressed using the Frumkin-Butler–Volmer theory in eqs 1 and 3

$$j_{acid}(E_{SHE}) = -2e_0 n_M \frac{c_{H^+}^{RP}}{c_{H^+}^{0}} A \times \exp\left[-\frac{\Delta G_{acidV}^{\neq,0} + \alpha_{acidV} F(E_{SHE} - \phi_{acid}^{RP} - E_{SHE,acidV}^{0})}{RT}\right] \quad (14)$$

E_{RHE} equals

$$E_{RHE} = E_{SHE} + RT/F \ln 10\ pH \quad (15)$$

Inserting eq 15 into eq 14 yields eqs 2 4

$$j_{acid}(E_{RHE}) = -2e_0 n_M \frac{c_{H^+}^{RP}}{c_{H^+}^{0}} A \times \exp\left[-\frac{\Delta G_{acidV}^{\neq,0} + \alpha_{acidV} F\left(E_{RHE} - \frac{RT}{F}\ln 10 pH_1 - \phi_{acid}^{RP} - E_{SHE,acidV}^{0}\right)}{RT}\right] \quad (16)$$

Similarly, the alkaline HER current density is obtained from eqs 2 and 4

$$j_{alka}(E_{SHE}) = -2e_0 n_M \frac{c_{H_2O}^{RP}}{c_{H_2O}^{0}} A \times \exp\left[-\frac{\Delta G_{alkaV}^{\neq,0} + \alpha_{alkaV} F(E_{SHE} - \phi_{alka}^{RP} - E_{SHE,alkaV}^{0})}{RT}\right] \quad (17)$$

which after inserting eq 15 gives

$$j_{alka}(E_{RHE}) = -2e_0 n_M \frac{c_{H_2O}^{RP}}{c_{H_2O}^{0}} \times A\exp\left[-\left[\Delta G_{alkaV}^{\neq,0} + \alpha_{alkaV} F\left(E_{RHE} - \frac{RT}{F}\ln 10\ pH_2 - \phi_{alka}^{RP} - E_{SHE,alkaV}^{0}\right)\right]/RT\right] \quad (18)$$

By solving the modified Poisson-Nernst–Planck Equation (eq 6) with the relevant boundary (eqs 16 or 18) and parameters (Tables 1, S1 and S2), j–E curves for HER at Au(111) can be

Table 1. Summary of the Key Parameters for HER at Au(111) in Acid and Alkaline and Their Temperature Dependency[a]

Temp	pH	$\Delta G_{acidV/alkaV}^{\neq,0}$ (eV)	$\alpha_{acidV/alkaV}$	$\phi_{acid/alka}^{RP}$ (V) −0.4 V_{RHE}	$E_{acidV/alkaV}^{0}$ (V_{SHE})	$\Delta G_{acidV/alkaV}^{\neq}$ (eV) −0.4 V_{RHE}
278 K	1	0.658	0.55	−0.148	−0.396	0.706
	13	0.575	0.38	−0.354	−1.210	0.745
283 K	1	0.660	0.55	−0.149	−0.399	0.711
	13	0.580	0.38	−0.359	−1.220	0.750
288 K	1	0.661	0.55	−0.150	−0.400	0.712
	13	0.588	0.39	−0.362	−1.224	0.761
293 K	1	0.662	0.55	−0.152	−0.402	0.715
	13	0.594	0.39	−0.368	−1.227	0.765
298 K	1	0.666	0.55	−0.153	−0.408	0.722
	13	0.602	0.41	−0.371	−1.236	0.782
303 K	1	0.667	0.55	−0.154	−0.412	0.725
	13	0.607	0.42	−0.373	−1.243	0.789
308 K	1	0.667	0.55	−0.155	−0.413	0.726
	13	0.612	0.42	−0.379	−1.248	0.793
313 K	1	0.668	0.55	−0.156	−0.414	0.727
	13	0.626	0.42	−0.384	−1.254	0.807

[a]The table provides the parameters with which the best fit is achieved for the experimental HER j–E curves and the microkinetic model at temperatures from 278 to 313 K.

https://doi.org/10.1021/prechem.4c00081
Precis. Chem. 2025, 3, 135–148

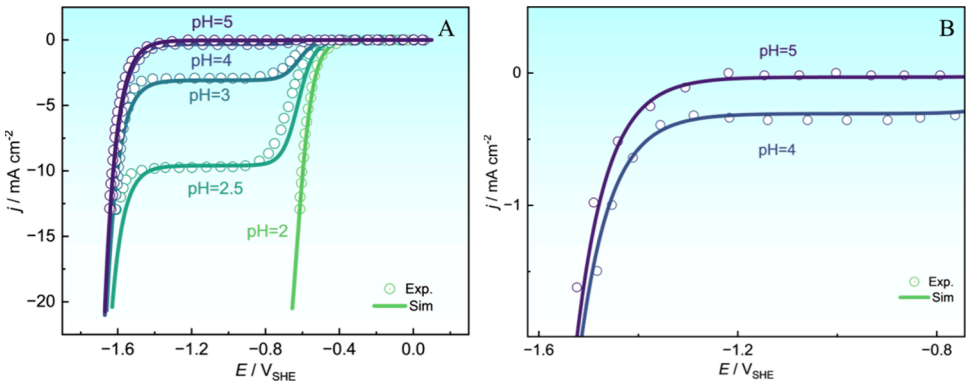

Figure 3. (A) Polarization curves given by the EDL model and experiments, and experimental data from the Markovic et al. group.[66] (B) A localized enlargement of Figure 3A.

obtained. A good agreement between the measured and simulated j–E curves for 0.1 M $HClO_4$ and 0.1 M NaOH can be seen in Figures 2A and 2B, respectively. The model parameters also lead to a satisfactory agreement with previous experimental data from different groups[66−71] on HER in 0.1 M $HClO_4$ and 0.1 M NaOH solutions as shown in Figures 2E and 2F.

The key parameters affecting the HER kinetics are listed in Table 1. At 298 K, $E^0_{SHE,acidV}$ is calculated based on the equation $E^0_{SHE,acidV} = -\Delta G^0_{H_{ad}}/e_0 = -(G^0_{H_{ad}} - G^0_{H^+})/e_0$, where $\Delta G^0_{H_{ad}}$ and $G^0_{H^+}$ are the adsorption free energy of hydrogen atom and Gibbs free energy for the formation of hydrated proton under standard equilibrium conditions of the acid HER, respectively. The free energy of an aqueous proton ($G^0_{H^+}$) on the SHE scale at pH = 0, $G^0_{H^+}$, is 0 eV. Correspondingly, at the same temperature, $E^0_{SHE,alkaV}$ is obtained from $E^0_{SHE,alkaV} = E^0_{SHE,acidV} - E^0_{H_2O}$, where $E^0_{H_2O}$ is the standard equilibrium potential of alkaline HER. At 298 K, $E^0_{SHE,acidV} = -0.408$ V because $\Delta G^0_{H_{ad}} = 0.408$ eV, whose value is close to what is predicted by DFT calculation by Santos et al.,[72] and $E^0_{SHE,alkaV} = -1.236$ V because $E^0_{H_2O} = -0.828$ V. The RP potential, $\phi^{RP}_{acid/alka}$, is obtained from the self-consistent solution of eqs 5 and 6.[36] $\Delta G^{\neq,0}_{acidV/alkaV}$ and $\alpha_{acidV/alkaV}$ are determined by fitting the measured j–E curves displayed in Figure 2A,B.

To further prove the credibility of the employed parameters, we simulated the polarization curves for pH ranging from 2 to 5 using the same model parameters listed in the Table 1 at 298 K and the HER kinetics (eqs 1 and 2), as shown in Figure 3A. Our model achieves good agreement with experimental results. This indicates two points. First, the developed hierarchical EDL model, the used reaction mechanism, and the selected model parameters used to describe pH-dependent HER are reasonable. Second, the proton discharge takes place more preferentially from hydronium ions than from water molecules. At lower pH values, eq 1 (j_{acid}) alone is sufficient to fit the experimental polarization curves for acidic HER, suggesting that hydrated protons discharge first. Between 2.5 ≤ pH ≤ 5, the total current is determined by the sum of eqs 1 and 2 ($j_{tot} = j_{acid} + j_{alka}$), which allows us to fit the experimental polarization curves. This indicates that protons are initially obtained from the hydronium, followed by the discharge of water molecules at higher overpotentials where the limiting diffusion current is observed. At pH = 13, eq 2 (j_{alka}) alone is sufficient to fit the alkaline HER curves, indicating that the water molecules are the dominant source of protons as the concentration of hydronium ions is too small to contribute even though there is discharge thermodynamically possible.

As the temperature is increased, the activation energy ($\Delta G^{\neq,0}_{acidV/alkaV}$) increases gradually and slight negative shift in the equilibrium potential $E^0_{SHE,acidV/alkaV}$ is seen at both pH = 1 and pH = 13. With the temperature rising from 278 to 313 K, $E^0_{SHE,acidV}$ ($E^0_{SHE,alkaV}$) decreases from −0.396 (−1.210) to −0.414 (−1.254) V_{SHE} and $\Delta G^{\neq,0}_{acidV}$($\Delta G^{\neq,0}_{alkaV}$) increases from 0.658 (0.575) to 0.668 (0.626) eV, respectively. This can be understood by the fact that on Au(111) the Volmer step R2 (R6) is an endothermic reaction with a negative reaction entropy of ca. -5.14×10^{-4} (-1.26×10^{-3}) eV/K (as estimated from $\Delta S^0_{acidV/alkaV} = e_0 \partial E^0_{SHE,acidV/alkaV}/\partial T$, following from Nernst equation) under standard equilibrium conditions. We have also tested other sets of parameters in the model to simulate the measured j–E curves but the experimentally measured HER current density ratio, $r_j(E_{RHE}) = \frac{j_{0.1\ M\ HClO_4}}{j_{0.1\ M\ NaOH}}$, is larger than unity in the entire potential −0.6 V < E_{RHE} < 0 V can be reproduced only when $\Delta G^{\neq,0}_{acidV} > \Delta G^{\neq,0}_{alkaV}$. The value obtained for $\Delta G^{\neq,0}_{acidV}$ is also in good agreement with DFT calculation by Santos et al.[2] Possible reasons for why $\Delta G^{\neq,0}_{acidV}$ is larger than $\Delta G^{\neq,0}_{alkaV}$ are discussed qualitatively in the following section.

From Table 1, it is evident that in the acidic HER, α_{acidV} after EDL correction remains relatively constant as the temperature increases, with a value of $\alpha_{acidV} \approx 0.55$. Conversely, in the alkaline HER, α_{alkaV} exhibits a slight increase with increasing temperature, and the approximate value of α_{alkaV} is 0.40, which is in agreement with previous reports of HER at Cu, Au, Pt, and Fe under similar reaction conditions.[73] These findings highlight the distinct pH and temperature dependencies of $\alpha_{acidV/alkaV}$ in acidic and alkaline environments.[73] Possible origin for the this will be discussed below.

From eqs 16 and 18 and the parameters given in Table 1, the smaller HER current in alkaline than in acid medium can be tentatively attributed to the slightly higher apparent activation energy in alkaline solutions. However, this does not necessarily mean that the intrinsic catalytic activity of HER in alkaline media would be smaller than in acid. In particular, the column 3 of Table 1 shows that in alkaline media the activation energy of the Volmer step is slightly smaller than that in acid when the overall HER is under standard equilibrium conditions. Instead, the higher apparent activation energy in 0.1 M NaOH than in $HClO_4$ results from the electrostatic effect; in alkaline solutions

https://doi.org/10.1021/prechem.4c00081
Precis. Chem. 2025, 3, 135−148

the electric potential at the RP is significantly more negative than in acidic solutions. Furthermore, the charge transfer coefficient in 0.1 M NaOH is also smaller. Together these two effects reduce the HER driving force as compared to acidic conditions and thereby make alkaline HER less active than the acidic even though the intrinsic reaction barrier in alkaline conditions is smaller than that in acidic solutions.

4.2. Possible Origins of the Smaller Standard Activation Energy and Charge Transfer Coefficients for the Volmer Reaction at Au(111) in Alkaline Media than That in Acid

According to the Schmicker-Koper-Santos (SKS) theory, the activation energy for forward Volmer reaction can be expressed as[74,75]

$$\Delta G^{\neq}_{\text{Volmer}} = E^{\text{el}}_{\text{cata}} + \frac{(e_0\eta + \lambda)^2}{4\lambda} \tag{19}$$

where $E^{\text{el}}_{\text{cata}} = \frac{\Delta^{\text{TS}}}{2\pi} \ln \frac{(\Delta^{\text{TS}})^2}{(\varepsilon_a(q^{\text{TS}}, d^{\text{TS}}) - \varepsilon_a^{\text{lb}})^2 + (\Delta^{\text{TS}})^2}$ describes the covalent interactions through the chemisorption function at the transition (Δ^{TS}) and the electronic energy of the hydrogen orbital at the transition state ($\varepsilon_a(q^{\text{TS}}, d^{\text{TS}})$). $\varepsilon_a^{\text{lb}}$ is the lower bound of the metal band and λ is the total reorganization free energy. eq 19 shows that both the solvent reorganization free energy and electrocatalytic effect contribute to the standard activation energy of the Volmer reaction. The total reorganization free energy λ includes contributions from both the solvent's inner- and outer-shell reorganization resulting from the proton transfer, $\lambda = \lambda_i + \lambda_o$. The inner-shell component can be treated within the harmonic approximation for the proton-related vibrations in the initial and final states[76] which allows writing

$$\lambda_i = \frac{m^*_H}{2}\omega_i\omega_f(x_i - x_f)^2 \tag{20}$$

where m^*_H is the effective mass of the transferring proton, and ω_i and ω_f are the vibrational frequencies in the initial state (hydronium ion in the acidic conditions (ν_{O-H^+}) or water molecule in the alkaline conditions (ν_{O-H}) and in the final state (chemisorbed hydrogen (ν_{Au-H}), respectively). x_i and x_f are the equilibrium positions of the proton in the initial and final state geometries, respectively. The outer-shell part can be obtained through dielectric continuum theory[77]

$$\lambda_o = \frac{1}{2\epsilon_0}\left(\frac{1}{\epsilon_\infty} - \frac{1}{\epsilon_s}\right)\int (D_i - D_f)^2 dV \tag{21}$$

where ϵ_0, ϵ_∞ and ϵ_S denote the vacuum permittivity, optical dielectric constant, and static dielectric constant, respectively. D_i and D_f refer to the electric displacement in the initial and final states, respectively, and can be determined from the corresponding charge density distributions. Due to the electrostatic screening effect, water molecules respond to the field and reorient to reduce the static dielectric constant near the electrode surface (ϵ_s near the electrode surface is much lower than in bulk solution, see eq 8).

Compared to the acidic condition, the reaction in the alkaline solution occurs at a potential range that is more negative than the PZFC. Therefore, under alkaline conditions the electrode surface bears a more negative charge which in turn attracts the H atoms in water molecules to be discharged closer to the electrode surface and makes x_i smaller in alkaline solutions than that in acidic solutions. Consequently, λ_i is smaller in the alkaline solution. Additionally, the stronger electric field near the electrode surface enhances the electrostatic screening effect in alkaline solutions, leading to a smaller value of λ_o.[78] Thus, the surface charge reduces both λ_i and λ_o components in alkaline solutions as compared to acidic solutions.

Besides changes in the reorganization energy, the Volmer barrier depends also on the covalent interactions. However, pH-dependent changes in this term are difficult to quantify as there are no DFT calculations on the barrier for formation of Au(111)-H bond via breaking of O−H bond. Nevertheless, we considered the pH-induced change in the covalent term, i.e. the catalytic effect, likely to be probably negligibly small due to the following facts: (i) the interaction between Au(111) and H is rather weak and its change with the amount of excess free charge (∼0.05 e) on Au(111) is rather small.[79] (ii) the Volmer reaction in both acid and alkaline media involves the breaking of O−H bond within the hydrogen bond network (HBN), the HBN makes the difference of free energy and related barrier rather small in the two media.[29] Hence, the pH-induced change of solvent reorganization free energy is probably the origin for why $\Delta G^{\neq,0}_{\text{alkaV}}$ is smaller than $\Delta G^{\neq,0}_{\text{acidV}}$ (eq 19 when $\eta = 0$), which may be rationalized by the decrease in the solvent reorganization free energy under higher electric field.[78,80] Another possible factor is the participation of cations in the alkaline HER and their effect on HER kinetics. The EDL model used herein does implicitly account for the role of cations within the EDL as it is possible to quantitatively calculate the changes in the Na^+ ions concentration as a function of potential and distance, as illustrated in Figure S6A and B. The Na^+ concentration can reach up to ∼3 M at −0.5 V_{RHE}. The interfacial OH^- concentration is vanishingly small, as shown in Figure S6C and D, and its influence on the HER can be considered negligible within the potential range studied in this work.

The high concentration of interfacial cations leads to two opposing effects: a promotional effect where cations activate water molecules within the EDL through the stabilization of reacting water molecules[81] and an inhibitory effect due to the high concentration of cations hindering the rate of proton migration toward the interface.[69] The latter influences the prefactor by controlling the reactant concentrations while the former may reduce the reaction and barrier free energies. However, cation-induced changes on the reaction and barrier free energies cannot be separated from reorganization free energy within our model (eq 19). More generally, within Marcus- or Schmickler-like theories cation-induced changes in either reaction and/or the barrier can be mapped as changes in the solvent reorganization free energy. In particular, the cation-coupled electron transfer model by Koper[81] gives the following activation energy for a reaction where electron transfer is influenced by cations:

$$\Delta G_{\text{act}} = \frac{(\lambda + D + \eta - \varphi_{\text{cation}})^2}{4(\lambda + D)} + \frac{\Delta^{\text{TS}}}{2\pi}\ln\frac{(\Delta^{\text{TS}})^2}{(\lambda + D + \eta - \varphi_{\text{cation}})^2 + (\Delta^{\text{TS}})^2} \tag{22}$$

where D is the bond dissociation energy, η is the overpotential, and φ_{cation} accounts for the direct cation-reactant interaction. Notably, the reorganization energy and the direction cation effect occur together and hence they cannot be separated unambiguously by measuring or simulating reaction kinetics or barriers. Therefore, either direct cation effects or the electro-

https://doi.org/10.1021/prechem.4c00081
Precis. Chem. 2025, 3, 135−148

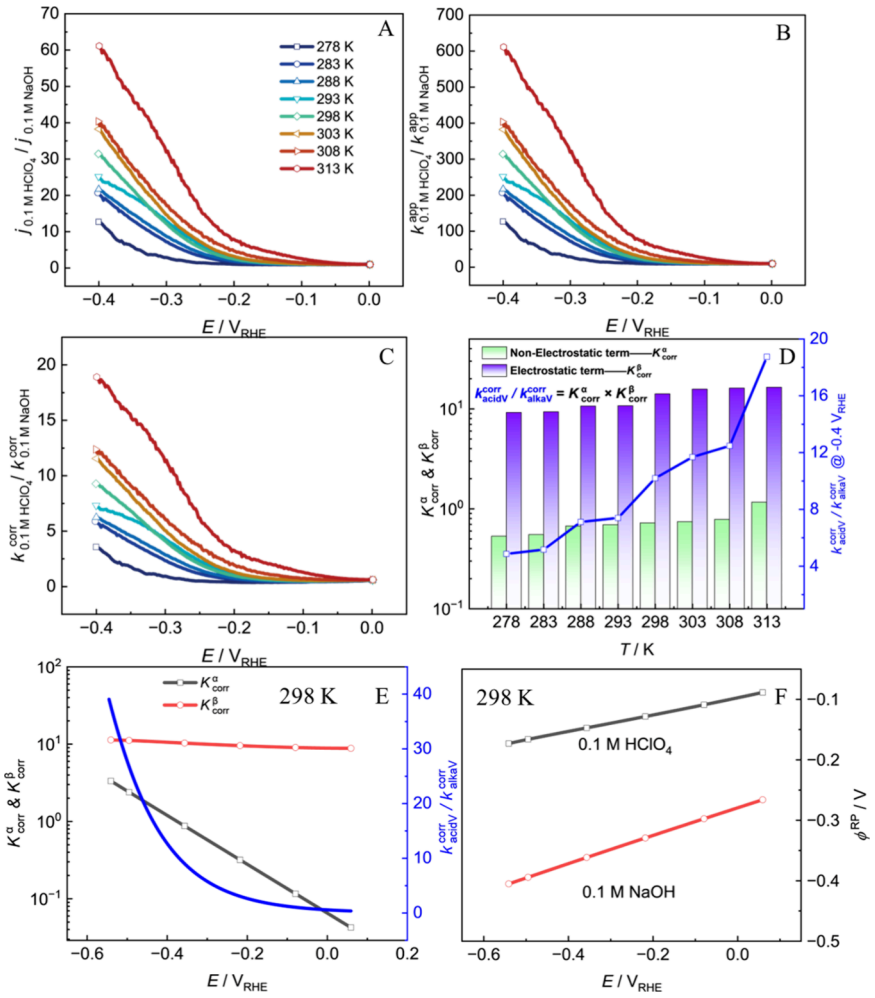

Figure 4. Ratio of (A) $j_{0.1\ M\ HClO_4}/j_{0.1\ M\ NaOH}$, r_j, (B) $k^{app}_{0.1\ M\ HClO_4}/k^{app}_{0.1\ M\ NaOH}$, r_k^{app}, and (C) $k^{corr}_{0.1\ M\ HClO_4}/k^{corr}_{0.1\ M\ NaOH}$, r_k^{corr}, at different temperatures as a function of potential in Ar-saturated 0.1 M $HClO_4$ and 0.1 M NaOH solutions. In this study, $k^{app}_{0.1\ M\ HClO_4} = \frac{j_{0.1\ M\ HClO_4}}{-2e_0 n_M c^{bulk}_{H^+}/c^0_{H^+}}$ and $k^{app}_{0.1\ M\ NaOH} = \frac{j_{0.1\ M\ NaOH}}{-2e_0 n_M c^{bulk}_{H_2O}/c^0_{H_2O}}$, $k^{corr}_{0.1\ M\ HClO_4} = \frac{j_{0.1\ M\ HClO_4}}{-2e_0 n_M c^{RP}_{H^+}/c^0_{H^+}}$ and $k^{corr}_{0.1\ M\ NaOH} = \frac{j_{0.1\ M\ NaOH}}{-2e_0 n_M c^{RP}_{H_2O}/c^0_{H_2O}}$, where $c^{RP}_{H^+}$ is calculated by solving the modified Poisson-Nernst−Planck equation and $c^{bulk}_{H_2O}$ is roughly assumed to $c^{bulk}_{H_2}$. (D) The nonelectrostatic term K^{α}_{corr}, electrostatic term K^{β}_{corr}, and r_k^{corr} at −0.4 V_{RHE} as a function of temperature. (E) K^{α}_{corr}, K^{β}_{corr} and $k^{corr}_{acidV}/k^{corr}_{alkaV}$ at 298 K as a function of electrode potential, calculated by eqs 29, 30 and 26, respectively. (F) Electric potential at the RP in 0.1 M $HClO_4$ and 0.1 M NaOH solutions at 298 K with electrode potential.

static effects in eq 19 will effectively manifest as lowering of the reorganization free energy, which is one of our key results; the lower intrinsic barrier under alkaline conditions ($\Delta G^{\neq,0}_{alkaV}$) compared to acidic solutions ($\Delta G^{\neq,0}_{acidV}$) is due to a smaller λ in alkaline solutions. The smaller λ might due to either φ_{cation} or electrostatic effects, but as the former has not been quantified and because our simulations directly show that the electrostatic interactions are significantly changed when going from the acidic to alkaline conditions, we consider that the decrease in λ is mainly due to electrostatic origin.

It is worth emphasizing again that the higher apparent activation Gibbs free energy for the Volmer reaction in base (last column in Table 1) mainly because of more negative potential at RP in alkaline medium than that in acidic medium, as seen in Figures S2B−C), results in more sluggish HER kinetics in base than in acid at Au(111), whose conclusion is similar to the previous work on pH-dependent HER kinetics using model Hamiltonian methods.[24]

On the other hand, assuming that the potential-dependent change of the first term in eq 19 is negligibly small, the charge transfer coefficient according to the eq 19 can be expressed as

$$\alpha_{acidV/alkaV} = \frac{1}{2} + \frac{F(E_{SHE} - E^0_{SHE,acidV/alkaV})}{2\lambda} \quad (23)$$

In the alkaline solution, the transfer coefficient, α_{alkaV}, is expected to be smaller than 0.5 when the applied potential is more negative than the equilibrium potential ($E^0_{SHE,\ alkaV} \approx -1.2$ V_{SHE}) of the Volmer reaction when the overall HER is under standard conditions (eq 23). Conversely, in the acidic solution, the transfer coefficient, α_{acidV}, will be larger than 0.5 when the applied potential is more positive than $E^0_{SHE,\ acidV} \approx -0.4$ V_{SHE}. The potential regime in acid and alkaline media examined in this work roughly agrees this relation. Moreover, the higher charge transfer coefficient for Volmer reaction in acid than that in base solution can be understood based on eq 23, λ is large, $\alpha \approx 0.5$. If λ is small, α deviates from 0.5. As we have discussed, λ is expected to be smaller in the alkaline solutions, which agrees

https://doi.org/10.1021/prechem.4c00081
Precis. Chem. 2025, 3, 135−148

well with the calculated transfer coefficient of alkaline solutions (~0.38−0.42).

4.3. Comparing Different Activity Metrics for Evaluating HER Activity and Its pH Dependence

The mostly commonly metric used for assessing HER activity is the exchange current density (j_0).[41,42] Herein, we analyze the quantitative difference of j_0 for HER at the Au(111) before and after EDL correction, i.e the prefactor in eqs 16 and 18. The j_0 of HER at Au(111) in acid and base obtained by extrapolating the Tafel plot is ca. $10^{-4.51} \sim 10^{-2.62}$ mA cm^{-2} and $10^{-3.24} \sim 10^{-2.66}$ mA cm^{-2}, respectively. The j_0 ratio in acid and base ranges between 0.05 and 1.10 at temperatures between 278 and 313 K, as seen in Figure S5 and Table S3. The exchange current density for HER in acidic media is smaller than that in alkaline media. This is probably a result of the extrapolation of the $j-E$ curves based on the Tafel analysis and assuming that the Tafel slope is constant with the change of electrode potential, which is not true in the lower overpotential region of HER as indicated in Figure 2C and 2D. Hence, caution must be exercised when using the extrapolation method to determine exchange current for comparative activity.[82]

Another commonly used activity metric is the ratio of the HER current density between the acidic and basic conditions at the same E_{RHE}, denoted as $r_j(E_{RHE}) = j_{0.1\ M\ HClO_4}/j_{0.1\ M\ NaOH}$, (Figure 4A). In the potential range with $-0.4\ V < E_{RHE} < -0.1\ V$, r_j is between 1 and ~60, depending on the applied potential and the reaction temperature. Since the (exchange) current density includes the contribution from concentration of reactants (eqs 1 and 2), it is better to compare the pH dependent rate constant for HER after eliminating the differences in the reactant concentrations (denoted as k_{app} hereafter) as widely adopted by experimentalists.[61] Commonly, the use of an excess of supporting electrolyte[83] has been used to rationalize the assumption that the surface concentration at the boundary of diffusion layer close to the metal electrode is the same as the bulk concentration of the reactants. In this study and the investigated potential regime, the surface proton surface is close to its bulk value because the HER kinetics at Au(111) are much smaller than the mass transport rate. The corresponding ratio of HER current density normalized by the concentration (activity) of bulk reactants in acidic and alkaline solutions, $r_k^{app} = \frac{j_{0.1\ M\ HClO_4}}{-2e_0 n_M c_{H^+}^{bulk}/c_{H^+}^0} \Big/ \frac{j_{(0.1\ M\ NaOH)}}{-2e_0 n_M c_{H_2O}^{bulk}/c_{H_2O}^0}$ is shown in Figure 4B.[84] Similar to r_j, r_k^{app} also increases as the E_{RHE} becomes more negative and rises as the temperature increases from 278 to 313 K. In the negative potential range of $-0.1\ V_{RHE}$ to $-0.4\ V_{RHE}$, r_k^{app} exhibits considerable variations, ranging from 1 to ~600 depending on the temperature.

In reality, however, the concentration of ionic reactant within the reaction volume or at the RP depend strongly on the excess surface free charge of the electrode and the following potential distribution within the EDL.[7,85] As a result, the bulk and local reactant concentrations at the boundary of diffusion layer close to the metal electrode may differ significantly and a proper estimation of $c_{H^+}^{RP}$ is necessary to obtain the correct intrinsic HER rate constant (denoted as $k_{0.1\ M\ HClO_4}^{corr} = \frac{j_{0.1\ M\ HClO_4}}{-2e_0 n_M c_{H^+}^{RP}/c_{H^+}^0}$ or $k_{0.1\ M\ NaOH}^{corr} = \frac{j_{0.1\ M\ NaOH}}{-2e_0 n_M c_{H_2O}^{RP}/c_{H_2O}^0}$ as referred from eqs 1 and 2). $c_{H^+}^{RP}$ at any potential, temperature and pH during HER at Au(111) can be calculated with the aid of the microkinetic simulations coupled with the modified PNP eq (eqs 5 and 6) based on the EDL model (Figure 1). The normalized current density ratios, correcting for the reactant concentration (activity) at the RP, $r_k^{corr} = k_{0.1\ M\ HClO_4}^{corr}/k_{0.1\ M\ NaOH}^{corr}$, as a function of potential are displayed in Figure 4C. r_k^{corr} exhibits a similar pH, potential and temperature trends as r_j, and r_k^{app}. however, the variations in concentration-corrected r_k^{corr} are significantly smaller, 1− ~ 18. Given that the apparent rate constant (r_k^{app}),the current density (r_j), and the corrected rate constant (r_k^{corr}) ratios differ significantly, one needs to be careful in choosing the most relevant activity metric. As the corrected rate constant ratio eliminates concentration effects, we consider it to be the most reliable metric for the *intrinsic* activity as a function of pH and temperature, instead of the apparent rate constant or current density commonly used.

The choice of the activity metric also impacts the obtained insight as can be seen by considering HER under kinetic control, where the apparent rate constant, $k^{app}(E_{RHE})$, and the corrected rate constant, $k^{corr}(E_{RHE})$, are

$$k_{acidV}^{app}(E_{RHE}) = \frac{c_{H^+}^{RP}}{c_{H^+}^{bulk}} A \exp\left[-\left[\Delta G_{acidV}^{\neq,0} + \alpha_{acidV} F\left(E_{RHE} - \frac{RT}{F} \ln 10\ pH_1 - \phi_{acid}^{RP} - E_{SHE,acidV}^0\right)\right]/RT\right] \quad (24)$$

$$k_{acidV}^{corr}(E_{RHE}) = A \exp\left[-\left[\Delta G_{acidV}^{\neq,0} + \alpha_{acidV} F \times \left(E_{RHE} - \frac{RT}{F} \ln 10\ pH_1 - \phi_{acid}^{RP} - E_{SHE,acidV}^0\right)\right]/RT\right] \quad (25)$$

$$k_{alkaV}^{app}(E_{RHE}) = A \exp\left[-\left[\Delta G_{alkaV}^{\neq,0} + \alpha_{alkaV} F \times \left(E_{RHE} - \frac{RT}{F} \ln 10\ pH_2 - \phi_{alka}^{RP} - E_{SHE,alkaV}^0\right)\right]/RT\right] \quad (26)$$

$k_{alkaV}^{app}(E_{RHE}) = k_{alkaV}^{corr}(E_{RHE})$ because $c_{H_2O}^{RP} = c_{H_2O}^{bulk}$.

To better analyze the data given in Figure 4, the kinetic equations are used to write analytic expressions of the rate constant and current density ratios at the same E_{RHE}, and to better analyze the data given in Figure 4. Dividing eq 25 by eq 26, we have

$$r_k^{corr} = \{\exp\{-[\Delta G_{acidV}^{\neq,0} + \alpha_{acidV} F(E_{RHE} - RT/F \ln 10\ pH_1 - \phi_{acid}^{RP} - E_{SHE,acidV}^0)]/RT\}\} / \{\exp\{-[\Delta G_{alkaV}^{\neq,0} + \alpha_{alkaV} F(E_{RHE} - RT/F \ln 10\ pH_2 - \phi_{alka}^{RP} - E_{SHE,alkaV}^0)]/RT\}\} \quad (27)$$

Dividing eq 24 by eq 26 we get

$$r_k^{app} = \frac{k_{acidV}^{app}(E_{RHE})}{k_{alkaV}^{app}(E_{RHE})} = r_k^{corr} \frac{c_{H^+}^{RP}}{c_{H^+}^{bulk}} \quad (28)$$

Dividing eq 16 by eq 18, we obtain

$$r_j = \frac{j_{acid}(E_{RHE})}{j_{alka}(E_{RHE})} = r_k^{app} \frac{c_{H^+}^{bulk}}{c_{H^+}^0} \Big/ \frac{c_{H_2O}^{RP}}{c_{H_2O}^0} \quad (29)$$

By comparing eqs 27-29, we can see that once we understand the factors controlling r_k^{corr} we can understand r_k^{app} and then r_j; the

https://doi.org/10.1021/prechem.4c00081
Precis. Chem. 2025, 3, 135−148

essence of the pH-dependent HER kinetics is contained in eq 27. For ease of analysis, eq 27 is further split into two parts, K^{α}_{corr} and K^{β}_{corr}. The nonelectrostatic term, K^{α}_{corr}, contains the differences in $\Delta G^{\neq,0}_{acidV/alkaV}$, $\alpha_{acidV/alkaV}$, pH and $E^{0}_{SHE,\ acidV/alkaV}$. The electrostatic term, K^{β}_{corr}, captures the contribution from differences in the RP electrostatic potential ($\phi^{RP}_{acid/alka}$). The equations describing these contributions are

$$K^{\alpha}_{corr} = \{\exp\{-[\Delta G^{\neq,0}_{acidV} + \alpha_{acidV}F(E_{RHE} - RT/F \ln 10\ pH_1 - E^{0}_{SHE,acidV})]/RT\}\} / \{\exp\{-[\Delta G^{\neq,0}_{alkaV} + \alpha_{alkaV}F(E_{RHE} - RT/F \ln 10\ pH_2 - E^{0}_{SHE,alkaV})]/RT\}\} \quad (30)$$

$$K^{\beta}_{corr} = \frac{\exp(\alpha_{acidV}F\phi^{RP}_{acid}/RT)}{\exp(\alpha_{alkaV}F\phi^{RP}_{alka}/RT)} \quad (31)$$

By using the data measured at 313 K and −0.4 V_{RHE} as an example, we provide a detailed elucidation of the multiple factors contributing to the observed r^{corr}_{k} with a net value of ∼18. At this potential, $\Delta G^{\neq,0}_{acidV}$ = 0.668 eV, $\Delta G^{\neq,0}_{alkaV}$ = 0.626 eV, α_{acidV} = 0.55, α_{alkaV} = 0.42, $E^{0}_{SHE,\ acidV}$ = −0.414 V, $E^{0}_{SHE,\ alkaV}$ = −1.254 V. Inserting these values in eq 30, gives $K^{\alpha}_{corr} \approx 1.16$. The corresponding RP electrostatic potentials are $\phi^{RP}_{acid}(-0.4\ V_{RHE})$ = −0.156 V, $\phi^{RP}_{alka}(-0.4\ V_{RHE})$ = −0.384 V, which entered in eq 31, give $K^{\beta}_{corr} \approx 16$. Therefore, $r^{corr}_{k}(-0.4\ V_{RHE}) = K^{\alpha}_{corr} * K^{\beta}_{corr} \approx 18$ (eq 27). The electrostatic term K^{β}_{corr} clearly determines the pH-dependent kinetics of the HER; the electrostatic potential differences at the RP are the underlying reason why the intrinsic HER kinetics are faster in acidic solutions than in alkaline solutions. More precisely, the electric potential at the RP ϕ^{RP}_{acid} in acidic solution is 0.227 V higher than ϕ^{RP}_{alka} in alkaline solution, making $K^{\beta}_{corr} \approx 16$, which is the main and important reason why the intrinsic kinetics of acidic HER is faster than that of alkaline HER at Au(111). After correcting for the EDL effects, the nonelectrostatic effects captured by K^{α}_{corr} are only weakly pH-dependent. K^{α}_{corr} and K^{β}_{corr} at −0.4 V_{RHE} in acidic and alkaline media at other temperatures are similar to those at 313 K, as shown in Figure 4D.

Different from $r^{corr}_{k}(-0.4\ V_{RHE}) \approx 18$, at the same potential and temperature, r^{app}_{k} is ∼600. This is because, in addition to the contributions of r^{corr}_{k}, ϕ^{RP}_{acid} results in an exponential growth in the concentration of hydronium ions and increases $c^{RP}_{H^+}/c^{bulk}_{H^+}$ by a factor of ∼33 (eq 28). Building upon r^{app}_{k}, r_j considers the disparity in concentration between the bulk reactant, hydronium and water molecules, where $c^{bulk}_{H^+}/c^{0}_{H^+}$ = 0.1 and $c^{RP}_{H_2O}/c^{0}_{H_2O}$ = 1. This leads to a 10-fold decrease in r_j relative to r^{app}_{k} (eq 29), resulting in $r_j \approx 60$, as illustrated in Figure 4A.

Figure 4E illustrates the evolution of K^{α}_{corr}, K^{β}_{corr}, and $k^{corr}_{acidV}/k^{corr}_{alkaV}$ (or r^{corr}_{k}) as a function of electrode potential at 298 K. Specifically, $k^{corr}_{acidV}/k^{corr}_{alkaV}$ ascends from close to 0 to nearly 40 as the electrode potential is decreased from 0 V_{RHE} to −0.55 V_{RHE}. In this progression, the electrostatic term, K^{β}_{corr}, grows by nearly an order of magnitude because the potential at the RP in acid solution is higher than that in alkaline solution (Figure 4F). In other words, the driving force for the HER in acid is greater than that in base at the same overpotential due to the electrostatic effect.

The nonelectrostatic term, K^{α}_{corr}, on the other hand, initially remains below 1 in the potential range from 0 V_{RHE} to −0.35 V_{RHE} but becomes slightly larger than 1 at more negative potentials. The value of below 1 in the low overpotential region is primarily attributed to the solvent reorganization free energy being smaller for alkaline than acidic HER at the same overpotential (eqs 20 and 21), which results in lower $\Delta G^{\neq,0}_{alkaV}$ than $\Delta G^{\neq,0}_{acidV}$ (Table 1). Conversely, $K^{\alpha}_{corr} > 1$ in the high overpotential region is mainly because the acidic electron transfer coefficient (α_{acidV}) is greater than the alkaline electron transfer coefficient (α_{alkaV}) (Table 1), which leads to a more pronounced reduction in the HER activation energy in acid with increasing overpotential.

In summary, the above analysis shows that under conditions where the HER mechanisms is identical in both acid and alkaline media, such as the present case for HER at Au(111), the ratio between the kinetic currents of HER in acidic and basic media entails contributions from the differences of reactant concentrations, EDL effects as well as the intrinsic reaction kinetics. Notably, each of these factors significantly affects the kinetic current density ratio and one should not put too much emphasis on a single factor, at least without carefully considering the other contributions. The EDL effects, encompassing the concentration and electrostatic potential at the RP, play a more prominent role for the HER at Au(111) studied herein. Our results show that in order to comprehend the ubiquitous pH effects observed for electrocatalytic proton coupled electron transfer reactions, it is necessary to select the proper activity metric, k_{corr}, rather than k_{app} or j. In particular, neither j and k_{app} should be used for evaluating the EDL effects on intrinsic kinetic activity, because both always and inherently depend the reactant concentration ratio which depends on the electrostatic potential. The corrected ratio k_{corr}, obtained using the EDL model, instead, informs about the intrinsic activity and shows that the higher apparent activation Gibbs free energy of the Volmer reaction in base is mainly because of the more negative potential at RP in alkaline medium than that in acidic medium, as seen in Figure 4F and Figures S2B−C); this is the main reason for the more sluggish HER kinetics in base than in acid at Au(111). However, the difference in activation energy is merely 40−80 meV, and the pH effect on the intrinsic kinetics is small. This in turn strongly implies that *performing EDL corrections is crucial before determining intrinsic activity.* Only by eliminating the interference of the EDL effect can experimental data better guide theoretical calculations toward more accurate results, and the free energy obtained from DFT calculations can more effectively reflect the intrinsic kinetics of the pH-dependent HER.

Before closing, we want to convey the idea that the pH-dependent kinetics of the HER is a multifaceted interaction of numerous factors, rather than a straightforward description encapsulated by a solitary descriptor, even for gold, a rather inert metal. While our results point out the importance electrostatic interactions and solvent reorganization free energy in modulating the intrinsic reaction rate, pH-dependent changes in the activation free energy and charge transfer coefficients, their temperature dependence in acid and alkaline media could be affected by other factors such as changes in the solvent structure or solvent polarization as discussed in ref.[86] Notably, all these are related to the solvent (reorganization) properties, which makes the careful computation of the reorganization free energy under relevant reaction conditions will be a crucial step in resolving the issue of pH effects in HER.

5. CONCLUSIONS

The hydrogen evolution reaction (HER) is a fundamental process in electrocatalysis with profound implications for energy conversion technologies. This study delved into the intricate

https://doi.org/10.1021/prechem.4c00081
Precis. Chem. 2025, 3, 135−148

pH-dependent kinetics of HER at the Au(111) electrode, shedding light on the multiple factors influencing this critical reaction. Our systematic investigation, in 0.1 M $HClO_4$ and 0.1 M NaOH solutions across a range of temperatures, uncovered multiple essential factors and key insights. First, we demonstrate that the impact of covalent bonding, i.e. the catalytic effect, electrostatic effect and concentration effect (mass transport) on the elementary step kinetics can be separated. This separation allowed us to scrutinize each factor separately and contrast commonly used activity metrics with each other; based on this detailed analysis we recommend the use of the corrected reaction constant as the most relevant metric for evaluating intrinsic HER kinetics, because it eliminates the impact of reactant concentrations, electric double-layer effects, and offers a holistic comprehension of pH-dependent intrinsic kinetics for electrocatalytic reactions.

We observed that, at identical overpotentials, the HER current ratio between pH = 1 and pH = 13, r_j, varies significantly with temperature, ranging from 1 up to approximately 60-fold. In contrast, the ratio between the corrected rate constants, r_k^{corr}resulting from the elimination of concentration effects and the electrostatic double layer effects, exhibits a much more modest variation between 1 and 20. The intrinsic standard activation energy for Volmer reaction in 0.1 M NaOH is ∼40−80 meV smaller than that in 0.1 M $HClO_4$, which is probably a result of smaller solvent reorganization free energy in alkaline solutions than that in acid due to the larger electric field and consequently smaller dielectric constant for the former case. Although the intrinsic activation energy is smaller in alkaline, the significantly more negative electric potential at RP in alkaline medium and the smaller charge transfer coefficient than that in acidic medium together lead to a higher apparent activation Gibbs free energy for the Volmer reaction and, consequently, slower HER kinetics in alkaline conditions.

While it needs to be acknowledged that significant future efforts are needed to develop a generally applicable theory of electrocatalysis and electrocatalytic reaction environment. The quantitative insight on the intrinsic catalytic activity, electrostatic effects, and concentration effects (mass transport) on the overall kinetics gained through the work herein will aid the rational design of electrocatalysts and optimization of electrochemical reaction conditions.

■ ASSOCIATED CONTENT

Supporting Information

The Supporting Information is available free of charge at https://pubs.acs.org/doi/10.1021/prechem.4c00081.

Detailed model parameters and results, including temperature-independent and temperature-dependent parameters used in the kinetic simulation and comprehensive computational workflow (Section I: Notes S1−S3, Figures S1, and Table S1−S2); additional details on the variation in hydronium concentration and electric potential within the double layer, base CV measurements at different temperatures, exchange current density, and distribution of anion and cation concentrations (Notes S4−S7, Figures S2−S6 and Table S3); possible origins for the difference in temperature-dependent electron transfer coefficients (Section II) (PDF)

■ AUTHOR INFORMATION

Corresponding Authors

Jun Huang − *Institute of Energy Technologies, IET3: Theory and Computation of Energy Materials, Forschungszentrum Jülich GmbH, 52425 Jülich, Germany;* orcid.org/0000-0002-1668-5361; Email: ju.huang@fz-juelich.de

Yan-Xia Chen − *Hefei National Research Center for Physical Sciences at Microscale, Department of Chemical Physics, University of Science and Technology of China, Hefei 230026, China;* orcid.org/0000-0002-1370-7422; Email: yachen@ustc.edu.cn

Authors

Er-Fei Zhen − *Hefei National Research Center for Physical Sciences at Microscale, Department of Chemical Physics, University of Science and Technology of China, Hefei 230026, China*

Bing-Yu Liu − *Hefei National Research Center for Physical Sciences at Microscale, Department of Chemical Physics, University of Science and Technology of China, Hefei 230026, China*

Meng-Ke Zhang − *Hefei National Research Center for Physical Sciences at Microscale, Department of Chemical Physics, University of Science and Technology of China, Hefei 230026, China*

Lu−Lu Zhang − *Institute of Energy Technologies, IET3: Theory and Computation of Energy Materials, Forschungszentrum Jülich GmbH, 52425 Jülich, Germany*

Chen-Yu Zhang − *Hefei National Research Center for Physical Sciences at Microscale, Department of Chemical Physics, University of Science and Technology of China, Hefei 230026, China*

Jun Cai − *Hefei National Research Center for Physical Sciences at Microscale, Department of Chemical Physics, University of Science and Technology of China, Hefei 230026, China*

Marko M. Melander − *Department of Chemistry, Nanoscience Center, University of Jyväskylä, FI-40014 Jyväskylä, Finland;* orcid.org/0000-0001-7111-1603

Complete contact information is available at: https://pubs.acs.org/10.1021/prechem.4c00081

Notes

The authors declare no competing financial interest.

■ ACKNOWLEDGMENTS

This work was supported by National Key R&D Program of China (2023YFA1509004) and National Natural Science Foundation of China (no. 22472162).

■ REFERENCES

(1) Frumkin, A. Hydrogen overvoltage. *Discuss. Faraday Soc.* **1947**, *1* (0), 57−67.

(2) Santos, E.; Lundin, A.; Pötting, K.; Quaino, P.; Schmickler, W. Model for the electrocatalysis of hydrogen evolution. *Phys. Rev. B* **2009**, *79* (23), No. 235436.

(3) Lam, Y.-C.; Soudackov, A. V.; Goldsmith, Z. K.; Hammes-Schiffer, S. Theory of Proton Discharge on Metal Electrodes: Electronically Adiabatic Model. *J. Phys. Chem. C* **2019**, *123* (19), 12335−12345.

(4) Inzelt, G. Milestones of the development of kinetics of electrode reactions. *J. Solid State Electr* **2011**, *15* (7), 1373−1389.

(5) Erdey-Grúz, T.; Volmer, M. Zur Theorie der Wasserstoff Überspannung. *Zeitschrift für Physikalische Chemie* **1930**, *150A* (1), 203−213.

(6) Volmer, M. Zur Theorie der Vorgänge an unpolarisierbaren Elektroden. *Zeitschrift für Physikalische Chemie* **1928**, *139A* (1), 597−604.
(7) Frumkin, A. N. Wasserstoffüberspannung und struktur der doppelschicht. *Zeitschrift für Physikalische Chemie* **1933**, *164* (1), 121−133.
(8) Trasatti, S. Work function, electronegativity, and electrochemical behaviour of metals: III. Electrolytic hydrogen evolution in acid solutions. *Journal of Electroanalytical Chemistry and Interfacial Electrochemistry* **1972**, *39* (1), 163−184.
(9) Nørskov, J. K.; Rossmeisl, J.; Logadottir, A.; Lindqvist, L.; Kitchin, J. R.; Bligaard, T.; Jonsson, H. Origin of the Overpotential for Oxygen Reduction at a Fuel-Cell Cathode. *J. Phys. Chem. B* **2004**, *108* (46), 17886−17892.
(10) Sheng, W.; Gasteiger, H. A.; Shao-Horn, Y. Hydrogen Oxidation and Evolution Reaction Kinetics on Platinum: Acid vs Alkaline Electrolytes. *J. Electrochem. Soc.* **2010**, *157* (11), B1529.
(11) Conway, B. E.; Bai, L. Determination of adsorption of OPD H species in the cathodic hydrogen evolution reaction at Pt in relation to electrocatalysis. *Journal of Electroanalytical Chemistry and Interfacial Electrochemistry* **1986**, *198* (1), 149−175.
(12) Subbaraman, R.; Tripkovic, D.; Strmcnik, D.; Chang, K.-C.; Uchimura, M.; Paulikas Arvydas, P.; Stamenkovic, V.; Markovic Nenad, M. Enhancing Hydrogen Evolution Activity in Water Splitting by Tailoring Li+-Ni(OH)2-Pt Interfaces. *Science* **2011**, *334* (6060), 1256−1260.
(13) Danilovic, N.; Subbaraman, R.; Strmcnik, D.; Chang, K.-C.; Paulikas, A. P.; Stamenkovic, V. R.; Markovic, N. M. Enhancing the Alkaline Hydrogen Evolution Reaction Activity through the Bifunctionality of Ni(OH)2/Metal Catalysts. *Angew. Chem., Int. Ed.* **2012**, *51* (50), 12495−12498.
(14) Jia, Q.; Liu, E.; Jiao, L.; Li, J.; Mukerjee, S. Current understandings of the sluggish kinetics of the hydrogen evolution and oxidation reactions in base. *Current Opinion in Electrochemistry* **2018**, *12*, 209−217.
(15) Rebollar, L.; Intikhab, S.; Oliveira, N. J.; Yan, Y.; Xu, B.; McCrum, I. T.; Snyder, J. D.; Tang, M. H. Beyond Adsorption. *Descriptors in Hydrogen Electrocatalysis. ACS Catalysis* **2020**, *10* (24), 14747−14762.
(16) Zheng, Y.; Jiao, Y.; Vasileff, A.; Qiao, S.-Z. The Hydrogen Evolution Reaction in Alkaline Solution: From Theory, Single Crystal Models, to Practical Electrocatalysts. *Angew. Chem., Int. Ed.* **2018**, *57* (26), 7568−7579.
(17) Durst, J.; Siebel, A.; Simon, C.; Hasché, F.; Herranz, J.; Gasteiger, H. A. New insights into the electrochemical hydrogen oxidation and evolution reaction mechanism. *Energy Environ. Sci.* **2014**, *7* (7), 2255−2260.
(18) Cheng, T.; Wang, L.; Merinov, B. V.; Goddard, W. A. Explanation of Dramatic pH-Dependence of Hydrogen Binding on Noble Metal Electrode: Greatly Weakened Water Adsorption at High pH. *J. Am. Chem. Soc.* **2018**, *140* (25), 7787−7790.
(19) Sheng, W.; Zhuang, Z.; Gao, M.; Zheng, J.; Chen, J. G.; Yan, Y. Correlating hydrogen oxidation and evolution activity on platinum at different pH with measured hydrogen binding energy. *Nat. Commun.* **2015**, *6* (1), 5848.
(20) Zheng, J.; Nash, J.; Xu, B.; Yan, Y. Perspective—Towards Establishing Apparent Hydrogen Binding Energy as the Descriptor for Hydrogen Oxidation/Evolution Reactions. *J. Electrochem. Soc.* **2018**, *165* (2), H27−H29.
(21) Zheng, J.; Sheng, W.; Zhuang, Z.; Xu, B.; Yan, Y. Universal dependence of hydrogen oxidation and evolution reaction activity of platinum-group metals on pH and hydrogen binding energy. *Science advances* **2016**, *2* (3), No. e1501602.
(22) Strmcnik, D.; Lopes, P. P.; Genorio, B.; Stamenkovic, V. R.; Markovic, N. M. Design principles for hydrogen evolution reaction catalyst materials. *Nano Energy* **2016**, *29*, 29−36.
(23) Lamoureux, P. S.; Singh, A. R.; Chan, K. pH Effects on Hydrogen Evolution and Oxidation over Pt(111): Insights from First-Principles. *ACS Catal.* **2019**, *9* (7), 6194−6201.
(24) Huang, J.; Li, P.; Chen, S. Quantitative Understanding of the Sluggish Kinetics of Hydrogen Reactions in Alkaline Media Based on a Microscopic Hamiltonian Model for the Volmer Step. *J. Phys. Chem. C* **2019**, *123* (28), 17325−17334.
(25) Govindarajan, N.; Xu, A.; Chan, K. How pH affects electrochemical processes. *Science (New York, N.Y.)* **2022**, *375* (6579), 379−380.
(26) Conway, B. E.; Wilkinson, D. F. Entropic and enthalpic components of the symmetry factor for electrochemical proton transfer from various proton donors over a wide temperature range. *Journal of Electroanalytical Chemistry and Interfacial Electrochemistry* **1986**, *214* (1), 633−653.
(27) Zeradjanin, A. R.; Polymeros, G.; Toparli, C.; Ledendecker, M.; Hodnik, N.; Erbe, A.; Rohwerder, M.; La Mantia, F. What is the trigger for the hydrogen evolution reaction?−towards electrocatalysis beyond the Sabatier principle. *Phys. Chem. Chem. Phys.* **2020**, *22* (16), 8768−8780.
(28) Ledezma-Yanez, I.; Wallace, W. D. Z.; Sebastián-Pascual, P.; Climent, V.; Feliu, J. M.; Koper, M. T. M. Interfacial water reorganization as a pH-dependent descriptor of the hydrogen evolution rate on platinum electrodes. *Nature Energy* **2017**, *2* (4), 17031.
(29) Li, P.; Jiang, Y.; Hu, Y.; Men, Y.; Liu, Y.; Cai, W.; Chen, S. Hydrogen bond network connectivity in the electric double layer dominates the kinetic pH effect in hydrogen electrocatalysis on Pt. *Nature Catalysis* **2022**, *5* (10), 900−911.
(30) Shen, L.-f.; Lu, B.-a.; Li, Y.-y.; Liu, J.; Huang-fu, Z.-c.; Peng, H.; Ye, J.-y.; Qu, X.-m.; Zhang, J.-m.; Li, G.; et al. Interfacial Structure of Water as a New Descriptor of the Hydrogen Evolution Reaction. *Angew. Chem., Int. Ed.* **2020**, *59* (50), 22397−22402.
(31) Frumkin, A. N.; Nikolaeva-Fedorovich, N. V.; Berezina, N. P.; Keis, K. E. The electroreduction of the S2O82−anion. *Journal of Electroanalytical Chemistry and Interfacial Electrochemistry* **1975**, *58* (1), 189−201.
(32) Fawcett, W. R. Fifty years of studies of double layer effects in electrode kinetics—a personal view. *J. Solid State Electrochem.* **2011**, *15* (7), 1347−1358.
(33) Huang, J.; Li, M.; Eslamibidgoli, M. J.; Eikerling, M.; Groß, A. Cation Overcrowding Effect on the Oxygen Evolution Reaction. *JACS Au* **2021**, *1* (10), 1752−1765.
(34) Ringe, S.; Clark, E. L.; Resasco, J.; Walton, A.; Seger, B.; Bell, A. T.; Chan, K. Understanding cation effects in electrochemical CO2 reduction. *Energy Environ. Sci.* **2019**, *12* (10), 3001−3014.
(35) Zhu, X.; Huang, J.; Eikerling, M. pH Effects in a Model Electrocatalytic Reaction Disentangled. *JACS Au* **2023**, *3* (4), 1052−1064.
(36) Zhang, L.; Cai, J.; Chen, Y.; Huang, J. Modelling electrocatalytic reactions with a concerted treatment of multistep electron transfer kinetics and local reaction conditions. *J. Phys.: Condens. Matter* **2021**, *33* (50), No. 504002.
(37) Qin, H.-G.; Li, F.-Z.; Du, Y.-F.; Yang, L.-F.; Wang, H.; Bai, Y.-Y.; Lin, M.; Gu, J. Quantitative Understanding of Cation Effects on the Electrochemical Reduction of CO2 and H+ in Acidic Solution. *ACS Catal.* **2023**, *13* (2), 916−926.
(38) Sheng, W.; Myint, M.; Chen, J. G.; Yan, Y. Correlating the hydrogen evolution reaction activity in alkaline electrolytes with the hydrogen binding energy on monometallic surfaces. *Energy Environ. Sci.* **2013**, *6* (5), 1509−1512.
(39) Strmcnik, D.; Uchimura, M.; Wang, C.; Subbaraman, R.; Danilovic, N.; van der Vliet, D.; Paulikas, A. P.; Stamenkovic, V. R.; Markovic, N. M. Improving the hydrogen oxidation reaction rate by promotion of hydroxyl adsorption. *Nat. Chem.* **2013**, *5* (4), 300−306.
(40) Zheng, Y.; Jiao, Y.; Zhu, Y.; Li, L. H.; Han, Y.; Chen, Y.; Jaroniec, M.; Qiao, S. Z. High Electrocatalytic Hydrogen Evolution Activity of an Anomalous Ruthenium Catalyst. *J. Am. Chem. Soc.* **2016**, *138* (49), 16174−16181.
(41) Durst, J.; Simon, C.; Siebel, A.; Rheinländer, P. J.; Schuler, T.; Hanzlik, M.; Herranz, J.; Hasché, F.; Gasteiger, H. A. (Invited) Hydrogen Oxidation and Evolution Reaction (HOR/HER) on Pt

Electrodes in Acid vs. Alkaline Electrolytes: Mechanism, Activity and Particle Size Effects. *ECS Trans.* **2014**, *64* (3), 1069.
(42) Durst, J.; Simon, C.; Hasché, F.; Gasteiger, H. A. Hydrogen Oxidation and Evolution Reaction Kinetics on Carbon Supported Pt, Ir, Rh, and Pd Electrocatalysts in Acidic Media. *J. Electrochem. Soc.* **2015**, *162* (1), F190.
(43) Lasia, A. Mechanism and kinetics of the hydrogen evolution reaction. *Int. J. Hydrogen Energy* **2019**, *44* (36), 19484−19518.
(44) Pentland, N.; Bockris, J. O. M.; Sheldon, E. Hydrogen Evolution Reaction on Copper, Gold, Molybdenum, Palladium, Rhodium, and Iron: Mechanism and Measurement Technique under High Purity Conditions. *J. Electrochem. Soc.* **1957**, *104* (3), 182.
(45) Gerischer, H.; Mehl, W. Zum Mechanismus der kathodischen Wasserstoffabscheidung an Quecksilber, Silber und Kupfer. *Zeitschrift für Elektrochemie, Berichte der Bunsengesellschaft für physikalische Chemie* **1955**, *59* (10), 1049−1059.
(46) Clavilier, J.; Faure, R.; Guinet, G.; Durand, R. Preparation of monocrystalline Pt microelectrodes and electrochemical study of the plane surfaces cut in the direction of the {111} and {110} planes. *J. Electroanal. Chem.* **1980**, *107* (1), 205−209.
(47) Chen, J.-Q.; Ye, X.-X.; Liao, L.-W.; Wei, Z.; Xu, M.-L.; Chen, Y.-X. Ohmic Drop Compensation in Electrochemical Measurement. *Journal of Electrochemistry* **2021**, *27* (3), 291−300.
(48) Uwitonze, N.; Chen, W.; Zhou, D.; He, Z.; Chen, Y.-X. The determination of thermal junction potential difference. *Science China Chemistry* **2018**, *61* (8), 1020−1024.
(49) Gavaghan, D.; Feldberg, S. Extended electron transfer and the Frumkin correction. *Journal of Electroanalytical Chemistry - J. ELECTROANAL CHEM* **2000**, *491*, 103−110.
(50) Nazmutdinov, R. R.; Glukhov, D. V.; Petrii, O. A.; Tsirlina, G. A.; Botukhova, G. N. Contemporary understanding of the peroxodisulfate reduction at a mercury electrode. *J. Electroanal. Chem.* **2003**, *552*, 261−278.
(51) Bronsted, J. J. C. R. Acid and Basic Catalysis. *Chem. Rev.* **1928**, *5* (3), 231−338.
(52) Trasatti, S. The absolute electrode potential: an explanatory note (Recommendations 1986). *Pure Appl. Chem.* **1986**, *58* (7), 955−966.
(53) Bieg, B.; Chrzanowski, J. Electron chemical potential in the context of unconventional quantum model. *Appl. Surf. Sci.* **2018**, *461*, 78−82.
(54) Huang, J. Density-Potential Functional Theory of Electrochemical Double Layers: Calibration on the Ag(111)-KPF6 System and Parametric Analysis. *J. Chem. Theory Comput.* **2023**, *19* (3), 1003−1013.
(55) Lam, Y.-C.; Soudackov, A. V.; Hammes-Schiffer, S. Theory of Electrochemical Proton-Coupled Electron Transfer in Diabatic Vibronic Representation: Application to Proton Discharge on Metal Electrodes in Alkaline Solution. *J. Phys. Chem. C* **2020**, *124* (50), 27309−27322.
(56) Rousseau, B. J. G.; Lu, X.; Soudackov, A. V.; Suntivich, J.; Abruña, H.; Hammes-Schiffer, S. Theoretical Analysis of Hydrogen Underpotential Deposition on Pt(111) Under Alkaline Conditions. *J. Phys. Chem. C* **2024**, *128* (29), 12109−12120.
(57) Liu, B.-Y.; Zhen, E.-F.; Zhang, L.-L.; Cai, J.; Huang, J.; Chen, Y.-X. The pH-Induced Increase of the Rate Constant for HER at Au(111) in Acid Revealed by Combining Experiments and Kinetic Simulation. *Anal. Chem.* **2024**, *96* (1), 67−75.
(58) Liu, B.-Y.; Zhen, E.-F.; Chen, W.; Zhang, L.-L.; Cai, J.; Chen, Y.-X. The importance of properly correcting the electric double layer effect in unravelling the intrinsic kinetics of electrode reactions. *Nano Materials Science* **2024**, DOI: 10.1016/j.nanoms.2024.03.008.
(59) Bockris, J. M.; Devanathan, M.; Müller, K. On the structure of charged interfaces. In *Electrochemistry*; Elsevier, 1965; pp 832−863.
(60) Trasatti, S.; Lust, E. The Potential of Zero Charge. In *Modern Aspects of Electrochemistry*, White, R. E., Bockris, J. O. M., Conway, B. E., Eds.; Springer: US, 1999; pp 1−215.
(61) Bard, A. J.; Faulkner, L. R.; White, H. S. *Electrochemical methods: fundamentals and applications*; John Wiley & Sons, 2022.
(62) Punathil Meethal, R.; Saibi, R.; Srinivasan, R. Hydrogen evolution reaction on polycrystalline Au inverted rotating disc electrode in HClO4 and NaOH solutions. *Int. J. Hydrogen Energy* **2022**, *47* (31), 14304−14318.
(63) Jung, O.; Jackson, M. N.; Bisbey, R. P.; Kogan, N. E.; Surendranath, Y. Innocent buffers reveal the intrinsic pH- and coverage-dependent kinetics of the hydrogen evolution reaction on noble metals. *Joule* **2022**, *6* (2), 476−493.
(64) Kirowa-Eisner, E.; Schwarz, M.; Rosenblum, M.; Gileadi, E. Temperature dependence of the transfer coefficient for the hydrogen evolution reaction on the DME. *J. Electroanal. Chem.* **1995**, *381* (1), 29−37.
(65) Frese, U.; Schmickler, W. Temperature Dependence of the Proton-Discharge Reaction at Gold and Silver Electrodes. *Berichte der Bunsengesellschaft für physikalische Chemie* **1988**, *92* (11), 1412−1417.
(66) Strmcnik, D.; Uchimura, M.; Wang, C.; Subbaraman, R.; Danilovic, N.; van der Vliet, D.; Paulikas, A. P.; Stamenkovic, V. R.; Markovic, N. M. Improving the hydrogen oxidation reaction rate by promotion of hydroxyl adsorption. *Nat. Chem.* **2013**, *5* (4), 300−306.
(67) Hamelin, A.; Weaver, M. J. Dependence of the kinetics of proton reduction at gold electrodes on the surface cyrstallographic orientation. *Journal of electroanalytical chemistry and interfacial electrochemistry* **1987**, *223* (1−2), 171−184.
(68) Bender, J. T.; Petersen, A. S.; Østergaard, F. C.; Wood, M. A.; Heffernan, S. M. J.; Milliron, D. J.; Rossmeisl, J.; Resasco, J. Understanding Cation Effects on the Hydrogen Evolution Reaction. *ACS Energy Letters* **2023**, *8* (1), 657−665.
(69) Goyal, A.; Koper, M. T. M. The Interrelated Effect of Cations and Electrolyte pH on the Hydrogen Evolution Reaction on Gold Electrodes in Alkaline Media. *Angew. Chem., Int. Ed.* **2021**, *60* (24), 13452−13462.
(70) Xue, S.; Garlyyev, B.; Watzele, S.; Liang, Y.; Fichtner, J.; Pohl, M. D.; Bandarenka, A. S. Influence of alkali metal cations on the hydrogen evolution reaction activity of Pt, Ir, Au, and Ag electrodes in alkaline electrolytes. *ChemElectroChem.* **2018**, *5* (17), 2326−2329.
(71) Goyal, A.; Koper, M. T. M. Understanding the role of mass transport in tuning the hydrogen evolution kinetics on gold in alkaline media. *J. Chem. Phys.* **2021**, *155* (13) (acccessed 8/13/2024).
(72) Santos, E.; Schmickler, W. Models of Electron Transfer at Different Electrode Materials. *Chem. Rev.* **2022**, *122* (12), 10581−10598.
(73) Haghighat, S.; Dawlaty, J. M. pH Dependence of the Electron-Transfer Coefficient: Comparing a Model to Experiment for Hydrogen Evolution Reaction. *J. Phys. Chem. C* **2016**, *120* (50), 28489−28496.
(74) Santos, E.; Koper, M. T. M.; Schmickler, W. A model for bond-breaking electron transfer at metal electrodes. *Chem. Phys. Lett.* **2006**, *419* (4), 421−425.
(75) Schmickler, W. On the Theory of Electrocatalysis. In *Electrochemical Science for a Sustainable Society: A Tribute to John O'M Bockris*, Uosaki, K., Ed.; Springer International Publishing, 2017; pp 95−111.
(76) Schmickler, W. The transfer coefficient in proton transfer reactions. *Journal of Electroanalytical Chemistry and Interfacial Electrochemistry* **1990**, *284* (2), 269−277.
(77) Ulstrup, J. Temperature dependence of the transfer coefficient in electron and atom group transfer processes. *Electrochim. Acta* **1984**, *29* (10), 1377−1380.
(78) Huang, J. Mixed quantum-classical treatment of electron transfer at electrocatalytic interfaces: Theoretical framework and conceptual analysis. *J. Chem. Phys.* **2020**, *153* (16) (acccessed 3/4/2024).
(79) Huang, J.; Chen, S. Interplay between Covalent and Noncovalent Interactions in Electrocatalysis. *J. Phys. Chem. C* **2018**, *122* (47), 26910−26921.
(80) Wilson, J. C.; Caratzoulas, S.; Vlachos, D. G.; Yan, Y. Insights into solvent and surface charge effects on Volmer step kinetics on Pt (111). *Nat. Commun.* **2023**, *14* (1), 2384.
(81) Koper, M. T. Theory and kinetic modeling of electrochemical cation-coupled electron transfer reactions. *J. Solid State Electrochem.* **2024**, *28* (5), 1601−1606.

(82) Wan, C.; Ling, Y.; Wang, S.; Pu, H.; Huang, Y.; Duan, X. Unraveling and Resolving the Inconsistencies in Tafel Analysis for Hydrogen Evolution Reactions. *ACS Central Science* **2024**, *10* (3), 658−665.
(83) Zhang, M.-K.; Chen, W.; Xu, M.-L.; Wei, Z.; Zhou, D.; Cai, J.; Chen, Y.-X. How Buffers Resist Electrochemical Reaction-Induced pH Shift under a Rotating Disk Electrode Configuration. *Anal. Chem.* **2021**, 93 (4), 1976−1983.
(84) Chen, W.; Zhang, M.-K.; Liu, B.-Y.; Cai, J.; Chen, Y.-X. Challenges and recent progress in unraveling the intrinsic pH effect in electrocatalysis. *Current Opinion in Electrochemistry* **2022**, *34*, No. 101003.
(85) Chen, W.; Zhang, L.-L.; Wei, Z.; Zhang, M.-K.; Cai, J.; Chen, Y.-X. The electrostatic effect and its role in promoting electrocatalytic reactions by specifically adsorbed anions. *Phys. Chem. Chem. Phys.* **2023**, *25* (12), 8317−8330.
(86) Ringe, S. Cation effects on electrocatalytic reduction processes at the example of the hydrogen evolution reaction. *Current Opinion in Electrochemistry* **2023**, *39*, No. 101268.

https://doi.org/10.1021/prechem.4c00081
Precis. Chem. 2025, 3, 135−148